Iraqi Journal of Physics, 2024 *Vol. 22, No. 2, PP. 81-89*
https://doi.org/10.30723/ijp.v22i2.1239 *P-ISSN: 2070-4003*
E-ISSN: 2664-5548

Thermodynamic and Spectroscopic Properties Investigation of Coronene as a Function of the Number of Oxygen Atoms and Temperature via Density Functional Theory

Taif Talib Khalaf[1a*] and Mohammed T. Hussein[1b]
[1]*Department of Physics, College of Science, University of Baghdad, Baghdad, Iraq*
[b]E-mail: mohammedtake@gmail.com
[a*]Corresponding author: taif.taleb1604a@sc.uobaghdad.edu.iq

Abstract

The study focused on the thermodynamics characteristics such as (Gibbs free energy, heat capacity, entropy and enthalpy) and spectroscopic properties like (IR spectra, reduced masses, and force constant) of coronene (C_{24}) and reduced coronene oxide ($C_{24}O_X$) where X =1–5 as a function of number of oxygen atoms and temperature from (298-398) ^oK. Density functional theory was used in the methodology with the basis sets 6-311G** and the hybrid functional B3LYP (Becke, 3-parameters, Lee-Yang-Parr), utilizing the Gaussian 09W program. Gaussian view 05 was used as a complementary program to calculate the geometrical structures. The Gibbs free energy and enthalpy decrease (negative sign) with increased oxygen atoms and temperature, indicating an exergonic reaction. The entropy and heat capacity increased with the number of oxygen atoms and temperature. The spectroscopic characteristics were compared with experimental results, particularly the longitudinal optical modes of vibration for graphene and graphene oxide (1585 - 1582) cm^{-1}, which were in good agreement.

Article Info.

Keywords:
Coronene, Coronene Oxide, Thermodynamics, Spectroscopic Properties, DFT.

Article history:
Received: Feb. 08, 2024
Revised: Apr. 16, 2024
Accepted: May 03, 2024
Published: Jun. 01, 2024

1. Introduction

Graphite is a crystalline form of carbon where the atoms are set up in a hexagonal configuration. It is more stable than diamond at atmospheric temperature and pressure [1, 2]. Graphite is a three-dimensional material consisting of millions of graphene layers [3]. It has excellent lubricating properties due to weak secondary Van der Waals bonds between the graphite layers, leading to easy interplanar cleavage [4, 5]. Graphene is a carbon material with two dimensions [6, 7]. Graphene highly unusual physical characteristics have attracted attention because of its 2D honeycomb grid-shaped of just one layer of atoms of sp^2-bonded carbon atoms [8-10]. In 2004, two researchers at the University of Manchester, Professor Andre Geim and Professor Kostya Novoselov, isolated graphene from bulk graphite [11]. It is the basic building block for all graphitic forms 0D fullerenes, 1D nanotubes and 3D graphite are all derived from 2D graphene [12, 13]. The structure of Graphene can be addressed by transforming it into unique forms, such as nanoribbons and quantum dots (QDs), depending on their suitability [14-16]. Graphene, possessing an exceptional two-dimensional carbon structure, was considered a material with promise for gas sensing [17-19] because of its intriguing electrical, mechanical, and thermal characteristics in addition to its sizable specific surface areas. Lately, graphene has been employed as a promising building block to create graphene-based noble metal nanostructures [20]. Graphene oxide (GO) is a derivative of graphene that has been oxygenated. It can readily be exfoliated and dispersed in a variety of solvents, including water, and it has ample oxygen functional groups [21, 22]. Coronene ($C_{24}H_{12}$), which is composed of seven peri-fused benzene rings, is a unique polyaromatic hydrocarbon (PAH) molecule, also referred to as superbenzene and cyclobenzene [23-26]. It is naturally present in sedimentary rock and

can also be detected during the hydrocracking process in petroleum refining [27]. Graphene is often represented by Coronene $C_{24}H_{12}$ [28-30]. But to replicate the actual presence of oxygen in the air rather than the uncommon hydrogen, oxygen ($C_{24}O$-$C_{24}O_5$) instead of hydrogen is used. The resulting substance is a p-type semiconductor known as reduced coronene oxide [31, 32]. The electronic, optoelectronic, linear and nonlinear optical thermodynamic properties and UV–Vis spectrum of coronene and coronene substituted with chlorine using Time-Dependent Density-Functional Theory (TDDFT) were investigated [33]. Coronene, through Density Functional Theory (DFT) at the B3LYP (Becke, 3-parameters, Lee-Yang-Parr) functional with a 6-31G(d) basis set, was also investigated to study the effects of substituting carbon atoms with B, N, and O on the electronic structure, linear and nonlinear optical properties [34]. In our previous study, the electronic and spectroscopic properties of C_{24}, $C_{24}O_5$ and their interaction with NO_2 gas molecules using DFT with Gaussian 09W software program were investigated [35]. In the present work, the effect of temperature and the number of oxygen atoms on the geometric, spectroscopic and thermodynamics characteristics of coronene (C_{24}) and reduced coronene oxide ($C_{24}O_X$), where x=1-5, was studied, which is a very important nanostructure in optoelectronics devices.

2. Methodology

The DFT is the most dependable theory for comprehending the characteristics and structure of molecules and nanostructures. DFT has gained a reputation because of its strong match to experimental data. Among the most often used DFT methods is B3LYP [36-41]. It was discovered that B3LYP was better than other functional, which encouraged its utilization. Energy from exchange-correlation sources is combined with HF exchange in the hybrid functional B3LYP [42]. For light atoms such as C and O, 6-311G** basic states were adopted in this investigation [43, 44]. Scaling factors with a value of 0.967 were employed to account for the frequency of vibration [45, 46]. The geometric analysis was carried out using Gaussian View 05 software, while the computations were carried out using Gaussian 09W software [47, 48], as illustrated in Fig. 1.

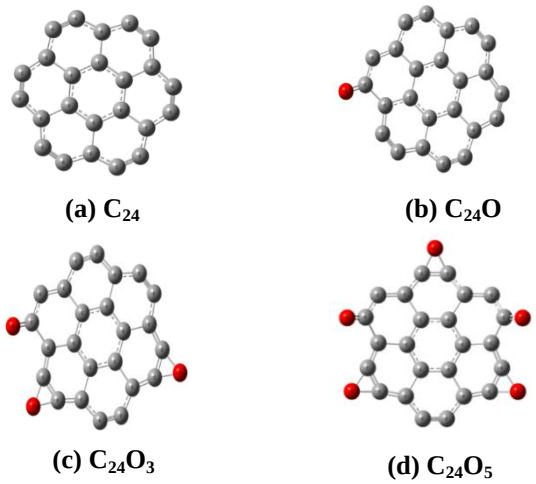

Figure 1: Geometrical optimization of (a) Coronene C_{24} and (b, c, d) reduced Coronene oxide ($C_{24}O$, $C_{24}O_3$, $C_{24}O_5$).

3. Results and Discussion

3.1. Thermodynamics Characteristics

Figs. 2 and 3 and Table 1 illustrate the variation of Gibbs free energy, enthalpy, entropy and heat capacity with the number of oxygen atoms at room temperature (298^{o}K). Figs. 4 and 5 and Table 2 show the thermodynamic properties of coronene C_{24} and reduced coronene oxide $C_{24}O$-$C_{24}O_5$ as a function of temperature between (298-398) ^{o}K. It was found that with increasing oxygen atoms, Gibbs free energy and enthalpy decreased in negative sign due to the increase in the size of the system and the increased interactions between the atoms. Increasing the temperature, Gibbs free energy change (**ΔG**) decreased according to Eq. 1, this behaviour is an exergonic reaction. Entropy and heat capacity increased with the increased number of oxygen atoms and temperature; this leads to increased disorder in the system with high temperature of the material, as shown in the following Eqs. 1 and 2 [49, 50]:

$$\Delta G = \Delta H - \Delta S \,.\, T \qquad (1)$$

where:
ΔH: Change in the enthalpy.
ΔS: Change in the entropy.
T: Temperature.

$$C = \frac{Q}{m \,.\, \Delta T} \qquad (2)$$

where: C is the heat capacity (J/(kg·K), Q is the amount of heat (in joules), m is the mass of the sample, and ΔT is the change between the starting and end temperatures.

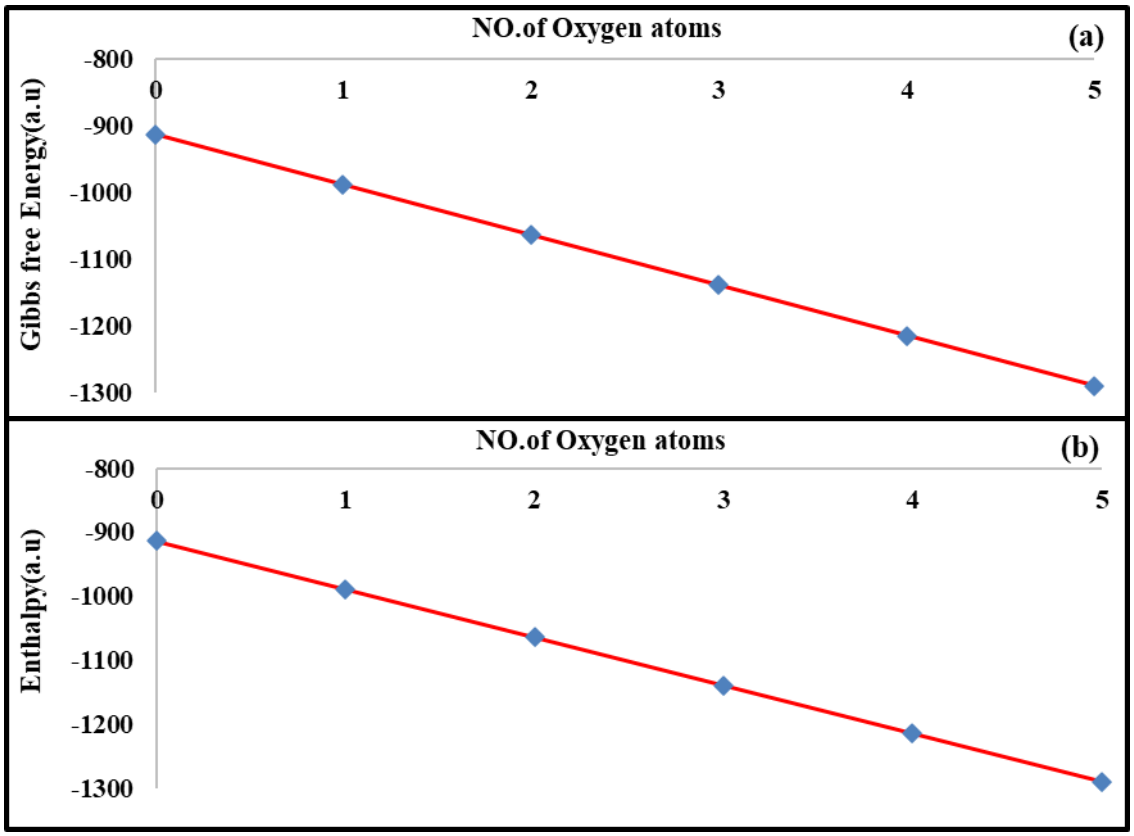

Figure 2: The thermodynamic properties of reduced Coronene oxide ($C_{24}O$-$C_{24}O_5$) compared with Coronene (C_{24}) for (a) Gibbs free energy and (b) enthalpy as a function of oxygen atoms.

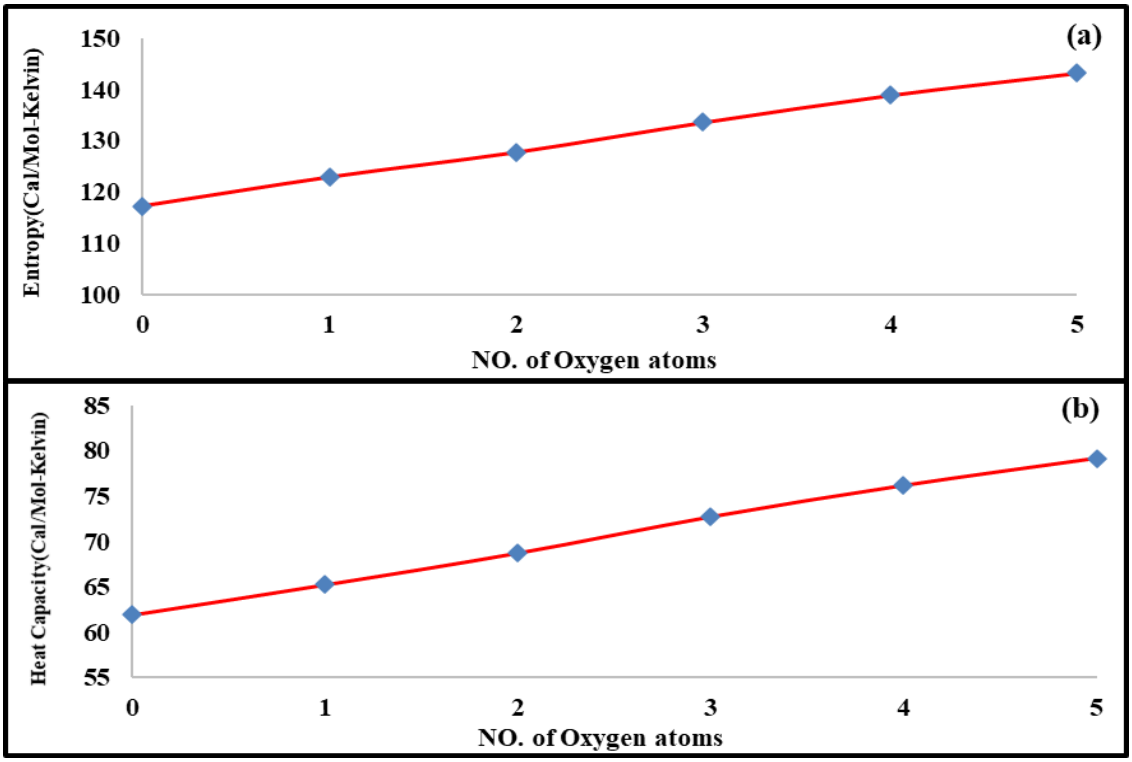

Figure 3: The thermodynamic properties of reduced Coronene oxide ($C_{24}O$-$C_{24}O_5$) compared with Coronene (C_{24}) for (a) entropy and (b) heat capacity as a function of oxygen atoms.

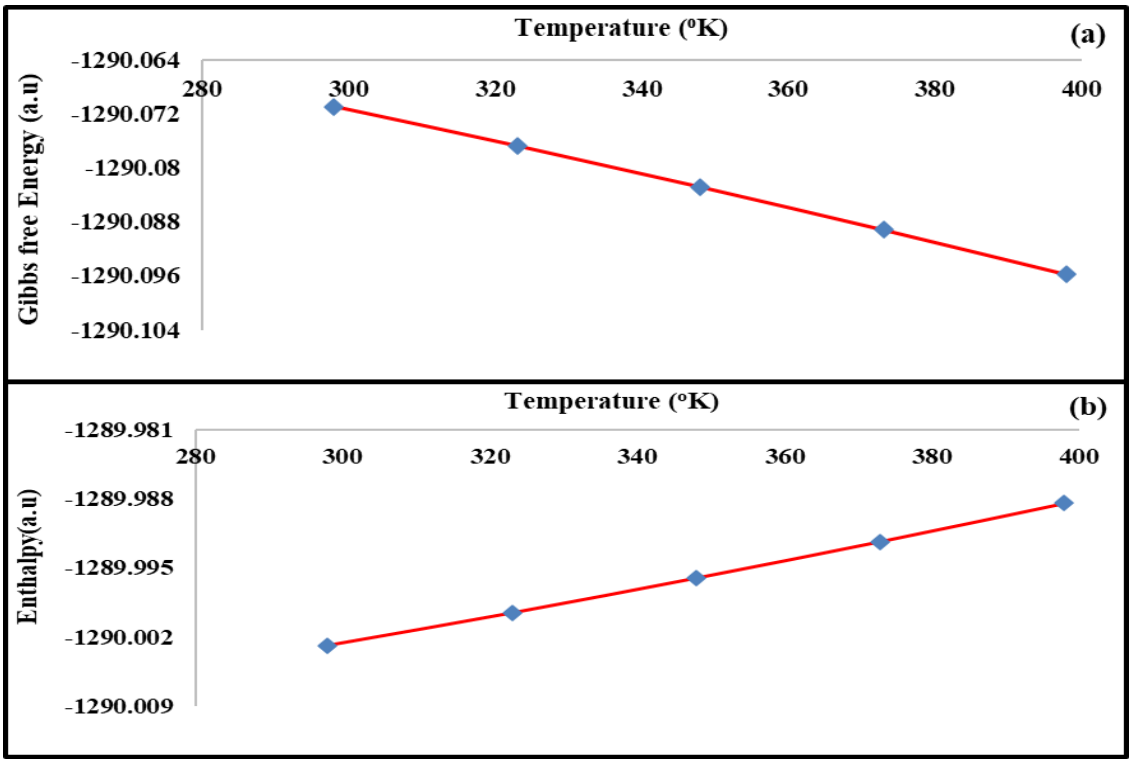

Figure 4: The thermodynamic properties of reduced Coronene oxide ($C_{24}O_5$) for (a) Gibbs free energy and (b) enthalpy as a function of temperatures.

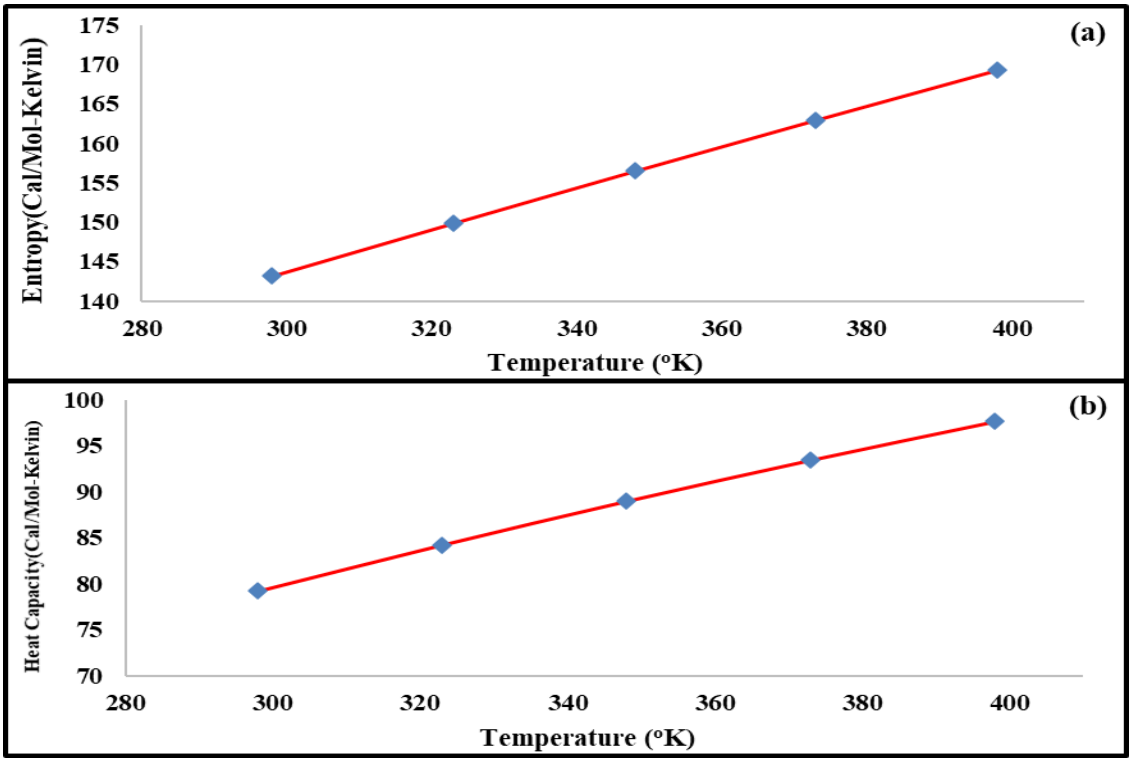

Figure 5: The thermodynamic properties of reduced Coronene oxide ($C_{24}O_5$) for (a) entropy and (b) heat capacity as a function of temperatures.

Table 1: the thermodynamic properties of C_{24} and $C_{24}O$-$C_{24}O_5$.

Thermodynamics properties	C_{24}	$C_{24}O$	$C_{24}O_2$	$C_{24}O_3$	$C_{24}O_4$	$C_{24}O_5$
ΔG (a.u)	-913.97	-989.20	-1064.41	-1139.62	-1214.85	-1290.07
ΔH (a.u)	-913.92	-989.14	-1064.35	-1139.55	-1214.79	-1290
ΔS (Cal/Mol-K)	117.25	122.91	127.76	133.57	138.86	143.20
CV (Cal/Mol-K)	61.92	65.25	68.74	72.74	76.20	79.19

Table 2: The thermodynamic properties of $C_{24}O_5$ at different temperature from (298-398) °K.

Thermodynamics properties	298 °K	323 °K	348 °K	373 °K	398 °K
ΔG (a.u)	-1290.070	-1290.076	-1290.082	-1290.089	-1290.095
ΔH (a.u)	-1290.002	-1289.999	-1289.996	-1289.992	-1289.988
ΔS (Cal/Mol-K)	143.20	149.90	156.50	162.97	169.30
CV (Cal/Mol-K)	79.19	84.22	88.98	93.46	97.65

3.2. Spectroscopic Properties

It can be noted from Fig. 6 and Table 3 that when the temperature was increased between 298 and 398 °K, the number of excited atoms increased according to Maxwell Boltzmann distribution, therefore the intensity of the IR spectra of the reduced coronene oxide ($C_{24}O_5$) increased accordingly. Fig. 7 exhibits the force constant and the reduced mass of the reduced coronene oxide ($C_{24}O_5$) as a function of frequency. Comparison with experimental data of Longitudinal Optical (LO) modes of vibration for graphene oxide 1582 cm^{-1} is included in the figures [51, 52]. The force constant as a function of frequency was represented by a parabola shape, while the reduced mass decreased with the increase of frequency according to Eq. 3 [53]:

$$\nu = \frac{1}{2\pi}\sqrt{\frac{k}{\mu}} \qquad (3)$$

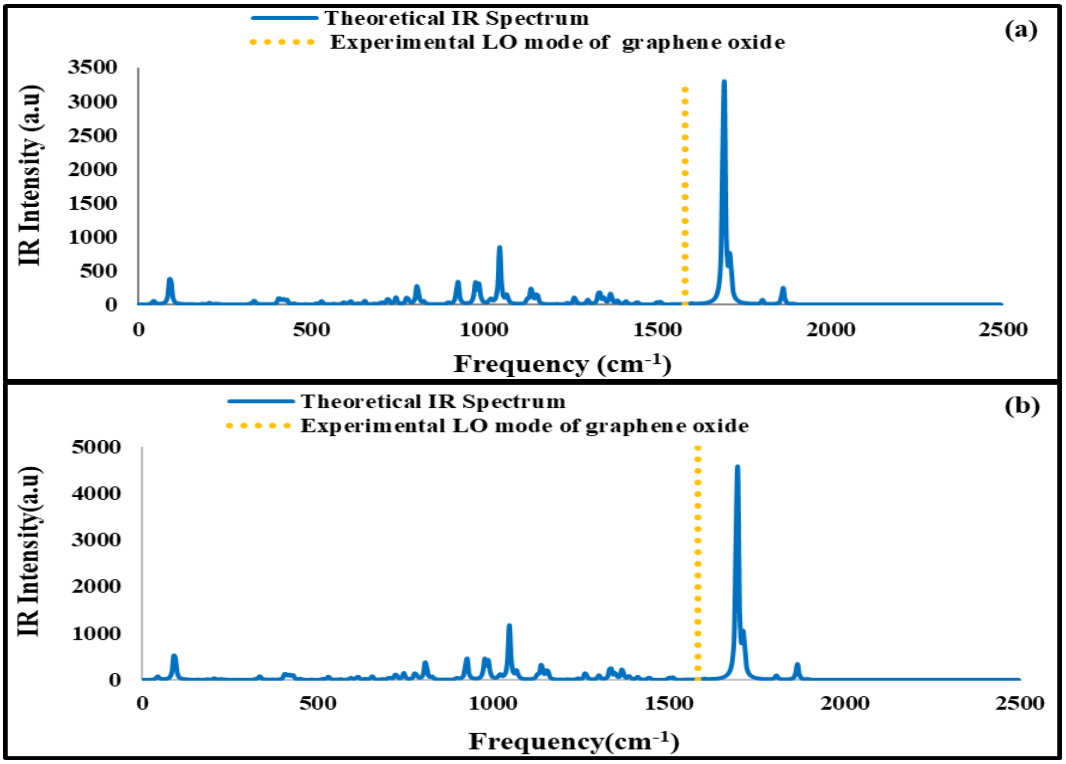

Figure 6: IR spectra for reduced Coronene oxide $C_{24}O_5$ as a function of frequency at (a) 298 ^{0}K and (b) 398 ^{0}K compared with experimental value of graphene oxide.

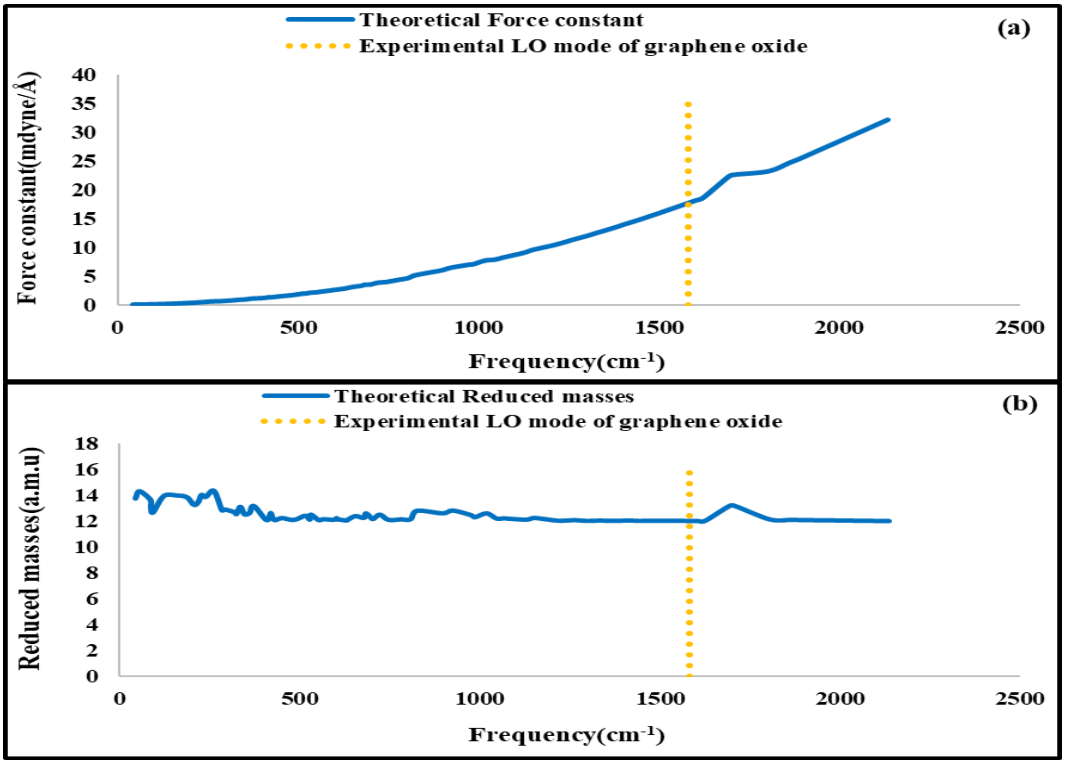

Figure 7: (a) Force constant and (b) Reduce mass for reduced coronene oxide $C_{24}O_5$ as a function of frequency compared with the experimental value of graphene oxide.

Table 3: The IR intensity and frequencies values of $C_{24}O_5$ at different temperature (298 and 398) ^{0}K.

Temperature (^{0}k)	IR Intensity (a.u)	Theoretical Frequency (cm^{-1})	Experimental Frequency (cm^{-1}) [51,52]
298 (^{o}K)	3264.46 (a.u)	1695 (cm^{-1})	1582 (cm^{-1})
398 (^{o}K)	4549.22 (a.u)	1695 (cm^{-1})	1582 (cm^{-1})

4. Conclusions

This work presented a theoretical study of coronene molecule C_{24} and reduced coronene oxide ($C_{24}O$-$C_{24}O_5$) using density functional theory with basis set 6-311G** and the hybrid functional (B3LYP). To calculate the thermodynamics properties, it was observed that Gibbs free energy decreased (in the negative sign) with the increase of temperature and number of oxygen atoms; this allows the conclusion that the material is exergonic. The spectroscopic properties of $C_{24}O_5$ were studied, and the intensity of IR absorption spectra of $C_{24}O_5$ increased with the increased temperature because there were more excited atoms. When the frequency of $C_{24}O_5$ increased, the reduced mass decreased while the force constant increased. These results were compared with experimental longitudinal optical modes of vibrations.

Acknowledgements

The authors would like to thank University of Baghdad, Collage of Science, Department of Physics.

Conflict of interest

Authors declare that they have no conflict of interest.

References

1. T. G. Vladkova, I. A. Ivanova, A. D. Staneva, M. G. Albu, A. S. Shalaby, T. I. Topousova, and A. S. Kostadinova, J. Arch. Mil. Med. **5**, e13223 (2017).
2. Y. Gao, J. Wu, X. Ren, X. Tan, T. Hayat, A. Alsaedi, C. Cheng, and C. Chen, Envir. Sci. Nano **4**, 1016 (2017).
3. H. Fallatah, M. Elhaneid, H. Ali-Boucetta, T. W. Overton, H. El Kadri, and K. Gkatzionis, Envir. Sci. Pollut. Res. **26**, 25057 (2019).
4. G. J. Simandl, S. Paradis, and C. Akam, British Columb. Minis. En. Min. British Columb. Geo. Sur. **3**, 163 (2015).
5. J. Li, X. Zeng, T. Ren, and E. Van Der Heide, Lubricants **2**, 137 (2014).
6. J. Cai, J. Tian, H. Gu, and Z. Guo, ES Mat. Manuf. **6**, 68 (2019).
7. H. Deng, J. Yin, J. Ma, J. Zhou, L. Zhang, L. Gao, and T. Jiao, Appl. Surf. Sci. **543**, 148821 (2021).
8. A. M. Pinto, I. C. Goncalves, and F. D. Magalhaes, Coll. Surf. B Biointer. **111**, 188 (2013).
9. E. Jennings, W. Montgomery, and P. Lerch, J. Phys. Chem. **114**, 15753 (2010).
10. S. M. Omran, E. T. Abdullah, and O. A. Al-Zuhairi, Iraqi J. Sci. **63**, 3719 (2022).
11. K. S. Novoselov, A. K. Geim, S. V. Morozov, D.-E. Jiang, Y. Zhang, S. V. Dubonos, I. V. Grigorieva, and A. A. Firsov, Science **306**, 666 (2004).
12. A. A. Menazea, H. A. Ezzat, W. Omara, O. H. Basyouni, S. A. Ibrahim, A. A. Mohamed, W. Tawfik, and M. A. Ibrahim, Comput. Theo. Chem. **1189**, 112980 (2020).
13. H. Liu and Y. Mao, ES Mat. Manuf. **13**, 3 (2021).

14. A. Marlinda, N. Yusoff, S. Sagadevan, and M. Johan, Int. J. Hydrog. En. **45**, 11976 (2020).
15. S. Sagadevan, Z. Z. Chowdhury, M. R. B. Johan, and R. F. Rafique, Mat. Res. Expr. **5**, 035014 (2018).
16. Y. Xu, K. Sheng, C. Li, and G. Shi, ACS Nano **4**, 4324 (2010).
17. D. Zhang, J. Liu, C. Jiang, A. Liu, and B. Xia, Sens. Act. B Chem. **240**, 55 (2017).
18. D. Zhang, Y. E. Sun, P. Li, and Y. Zhang, ACS Appl. Mat. Inter. **8**, 14142 (2016).
19. C. A. Zito, T. M. Perfecto, and D. P. Volanti, Sens. Act. B Chem. **244**, 466 (2017).
20. A. H. Mohammed and A. N. Naje, Iraqi J. Sci. **63**, 5218 (2022).
21. F. El-Hossary, A. Ghitas, A. Abd El-Rahman, M. A. Shahat, and M. H. Fawey, Vacuum **188**, 110158 (2021).
22. S. Park and R. Ruoff, Chem. Soc. Rev. **39**, 228 (2010).
23. J. C. Fetzer, *Large (C>= 24) Polycyclic Aromatic Hydrocarbons: Chemistry and Analysis* (USA, John Wiley & Sons, 2000).
24. F. R. Nikmaram, K. Kalateh, and P. Kanganizadeh, Int. J. New Chem. **1**, 160 (2014).
25. V. Zubkov, Geochem. Int. **47**, 741 (2009).
26. L. Allamandola, S. Sandford, and B. Wopenka, Science **237**, 56 (1987).
27. B. J. Frogley and L. J. Wright, Angewan. Chem. **129**, 149 (2017).
28. S. Prodhan, S. Mazumdar, and S. Ramasesha, Molecules **24**, 730 (2019).
29. M. F. Budyka, Spectrochim. Acta Part A Molec. Biomolec. Spect. **207**, 1 (2019).
30. B. Saha and P. K. Bhattacharyya, ACS Omega **3**, 16753 (2018).
31. S. Drewniak, Ł. Drewniak, and T. Pustelny, Sensors **22**, 5316 (2022).
32. D.-T. Phan and G.-S. Chung, J. Phys. Chem. Sol. **74**, 1509 (2013).
33. G. Ejuh, F. Tchangnwa Nya, N. Djongyang, and J. Ndjaka, SN Appl. Sci. **2**, 1 (2020).
34. M. El Masfioui, S. Bahsine, A. Elbiyaali, and F. Allali, E3S Web of Conferences (EDP Sciences, 2022). p. 00048.
35. S. K. Abdulradha, M. T. Hussein, and M. A. Abdulsattar, Int. J. Nanosci. **21**, 2250009 (2022).
36. E. Zins, M. Guinet, D. Rodriguez, and S. Payan, J. Quant. Spect. Rad. Tran. **283**, 108141 (2022).
37. M. A. Abdulsattar, Karbala Int. J. Mod. Sci. **6**, 13 (2020).
38. N. F. Jafer and M. T. Hussein, Int. J. Nanosci. **21**, 2250006 (2022).
39. N. Kerru, L. Gummidi, S. V. Bhaskaruni, S. N. Maddila, P. Singh, and S. B. Jonnalagadda, Sci. Rep. **9**, 19280 (2019).
40. F. A. Hasan and M. T. Hussein, Mat. Today Proce. **42**, 2638 (2021).
41. M. T. Hussein, Iraqi J. Phys. **15**, 54 (2017).
42. S. Tingting, Z. Fuchun, and Z. Weihu, Rar. Met. Mat. Eng. **44**, 2409 (2015).
43. M. A. Abdulsattar, H. H. Abed, R. H. Jabbar, and N. M. Almaroof, J. Molec. Graph. Mod. **102**, 107791 (2021).
44. P. Pal, A. Yadav, P. S. Chauhan, P. K. Parida, and A. Gupta, Sens. Int. **2**, 100072 (2021).
45. M. Hussein, T. Fayad, and M. Abdulsattar, Chalcogen. Lett. **16**, 557 (2019).
46. S. K. Abdulridha, M. A. Abdulsattar, and M. T. Hussein, Struct. Chem. **33**, 2033 (2022).
47. M. T. Hussein and H. A. Thjeel, Journal of Physics: Conference Series (IOP Publishing, 2019). p. 012015.
48. M. Frisch, G. Trucks, H. Schlegel, G. E. Scuseria, M. A. Robb, J. R. Cheeseman, J. Montgomery Jr, T. Vreven, K. Kudin, and J. Burant, *Gaussian 03, Revision c. 02, Gaussian* (Pittsburgh, PA, USA, Inc., Wallingford, CT, 2004).

49. C.-S. Jia, L.-H. Zhang, X.-L. Peng, J.-X. Luo, Y.-L. Zhao, J.-Y. Liu, J.-J. Guo, and L.-D. Tang, Chem. Eng. Sci. **202**, 70 (2019).
50. M. Popovic, G. B. Stenning, A. Göttlein, and M. Minceva, J. Biotech. **331**, 99 (2021).
51. A. Jorio, ISRN Nanotechnology **2012**, 1 (2012).
52. Y. Shen, S. Yang, P. Zhou, Q. Sun, P. Wang, L. Wan, J. Li, L. Chen, X. Wang, and S. Ding, Carbon **62**, 157 (2013).
53. W. Gao, Z. Li, and N. M. Sammes, *Introduction to Electronic Materials for Engineers* (Singapore, World Scientific Publishing Company, 2011).

دراسة الخصائص الحرارية والطيفية للكورونين كدالة لأعداد الاوكسجين والحرارة باستخدام نظرية دالية الكثافة

طيف طالب خلف[1] ومحمد تقي حسين[1]

[1] قسم الفيزياء، كلية العلوم، جامعة بغداد، بغداد، العراق

الخلاصة

في هذا البحث، ركزت الدراسة على الخصائص الحرارية مثل (طاقة جيبس الحرة، السعة الحرارية، الإنتروبي والإنثالبي) بالإضافة الى الخصائص الطيفية المتضمنة (اطياف الاشعة تحت الحمراء، الكتلة المختزلة وثابت القوة) للكورونين C_{24} والكورونين اوكسايد المختزل $C_{24}O_X$ حيث X=1–5 كدالة لعدد ذرات الاوكسجين ودرجة الحرارة من ^oK (298-398). تستخدم المنهجية الحالية نظرية دالية الكثافة DFT مع الدالة الهجينة B3LYP (Becke, 3-parameters, Lee-Yang-Parr) ومجموعة الاساس 6-311G** بأستخدام برنامج Gaussian 09W. تم حساب التراكيب الهندسية بأستخدام برنامج تكميلي Gaussian view 05. تتناقص طاقة جيبس الحرة والانثالبي (في اشارة سالبة) مع زيادة عدد ذرات الاوكسجين ودرجة الحرارة مما يدل على وجود تفاعل باعث للطاقة، بينما يزداد الإنتروبي والسعة الحرارية مع زيادة عدد ذرات الاوكسجين ودرجة الحرارة. تمت مقارنة الخصائص الطيفية مع النتائج العملية وتحديدا الانماط البصرية الطولية للاهتزاز للكرافين والكرافين اوكسايد cm^{-1} (1582 - 1585) والتي كانت متطابقة بشكل جيد.

الكلمات المفتاحية: الكورونين، الكورونين اوكسايد، الخصائص الحرارية، والطيفية، DFT.